Atmospheric Research 140–141 (2014) 85–94

Contents lists available at ScienceDirect

Atmospheric Research

journal homepage: www.elsevier.com/locate/atmos

Effect of off-zenith observations on reducing the impact of precipitation on ground-based microwave radiometer measurement accuracy

Guirong Xu [a,*], Randolph (Stick) Ware [b], Wengang Zhang [a], Guangliu Feng [a], Kewen Liao [c], Yibing Liu [c]

[a] Hubei Key Laboratory for Heavy Rain Monitoring and Warning Research, Institute of Heavy Rain, China Meteorological Administration, Wuhan 430074, China
[b] Radiometrics, 4909 Nautilus Court North, Boulder, CO, USA
[c] Wuhan Meteorological Bureau of Hubei Province, Wuhan 430040, China

ARTICLE INFO

Article history:
Received 8 November 2013
Received in revised form 20 January 2014
Accepted 27 January 2014
Available online 31 January 2014

Keywords:
Microwave radiometer
Off-zenith observation
Precipitation
Accuracy

ABSTRACT

Microwave radiometers (MWRs) can be useful for the detection of mesoscale phenomena because they provide thermodynamic profiles in a minute time scale. These profiles are mainly used in non-precipitation conditions due to degraded accuracy of the MWR measurements in precipitation. Recently, Radiometrics Corporation used proprietary neural network methods to retrieve temperature, humidity and liquid profiles from off-zenith (15° elevation) radiometer observations to provide higher accuracy during precipitation. In this paper, using the MWR-retrieved temperature and humidity profiles with collocated radiosondes from June 2010 to September 2013 in Wuhan, the impact of precipitation on the MWR measurement accuracy as well as the effect of off-zenith neural network methods on it is investigated. In precipitation, the correlation coefficients of the MWR temperature and vapor density profiles against radiosondes are smaller than those in non-precipitation, and the bias and RMS against radiosondes also increase, especially around 2 km heights. For the MWR relative humidity profile, the correlation coefficient in precipitation is obvious smaller than that in non-precipitation below 4.5 km, and the bias and RMS against radiosondes are clearly larger above 5.5 km. Moreover, the differences between the precipitation and non-precipitation cases mostly are statistically significant. Compared with the results of the zenith observation, the off-zenith observation makes a positive effect on reducing the impact of precipitation on the accuracy of MWR temperature and vapor density retrievals. On the whole, the MWR temperature bias and RMS against radiosondes in precipitation are reduced from 3.6 and 4.2 K to 1.3 and 3.1 K, respectively, and the MWR vapor density bias is also reduced from 1.10 g/m^3 to 0.18 g/m^3 with the RMS decreasing from 2.90 g/m^3 to 1.91 g/m^3. The temperature correlation coefficient between the MWR and radiosonde in precipitation is clearly improved above 3 km heights, and the temperature bias and RMS are significantly reduced at most heights. For the MWR vapor density retrievals in precipitation, the correlation coefficient, bias and RMS against radiosondes are clearly improved above 2 km heights. Additionally, the off-zenith observations during non-precipitation cases are also better compared to zenith observations. Therefore, off-zenith observations generally are better than zenith observations. This could be due to the fact that the off-zenith observations are more representative of the conditions in which radiosonde observations are also taken.

* Corresponding author at: Institute of Heavy Rain, China Meteorological Administration No. 3 Donghudong Road, Wuhan 430074, Hubei, China. Tel.: +862767847954; fax: +862787806597.
E-mail addresses: grxu@whihr.com.cn, grxu2007@gmail.com (G. Xu).

0169-8095/$ – see front matter © 2014 Elsevier B.V. All rights reserved.
http://dx.doi.org/10.1016/j.atmosres.2014.01.021

1. Introduction

Atmospheric temperature and humidity profiles are significant for meteorological research and commonly obtained with traditional radiosondes, which are launched only twice each day in operation. Many of the meteorological phenomena occurring at mesoscale require observations sufficiently close together in time and space. However, the lack of observations necessary to define mesoscale systems is a critical meteorological problem. Ground-based microwave radiometers (MWRs) retrieve the temperature, humidity and liquid profiles up to 10 km by measuring the radiation intensity at a number of frequency channels in the microwave spectrum that are dominated by atmospheric water vapor, cloud liquid water and molecular oxygen emissions. These profiles are available nearly continuously, at intervals of several minutes (Chan, 2009). The high temporal resolution is able to resolve detailed mesoscale thermodynamic and limited microphysical features of various rapidly changing mesoscale and/or hazardous weather phenomena (Knupp et al., 2009). In addition, continuous time series of traditional forecast indices generated from MWR data can be combined algorithmically to predict early stage convection hours before it is detected by widely used electric field mill convective prediction methods (Madhulatha et al., 2013). Over the past decade MWRs are installed in many countries and applied in nowcasting convective activity, data assimilation, and climate studies (Liu et al., 2009; Chan and Hon, 2011; Cimini et al., 2011; Spänkuch et al., 2011; Xie et al., 2011; Tang et al., 2012; Cadeddu et al., 2013; Huang et al., 2013; Madhulatha et al., 2013; Raju et al., 2013; Venkat Ratnam et al., 2013; Ware et al., 2013).

Continuous MWR measurements can be very useful for the detection of mesoscale phenomena that require very high spatial and temporal scales. Twice-daily radiosonde data are commonly used to generate Stability Indices for lightning, rain, hail and gusty wind prediction several hours in advance. However, several hours after launch the radiosonde data typically become stale and ineffective. In contrast, a MWR provides continuous thermodynamic soundings from which continuous Stability Indices can be generated. The resulting Stability Index time series provide promising new tools for local high-impact weather forecasting. For example, lightning prediction of more than 2 h in advance is reported using an algorithm that combines Stability Index time series (Madhulatha et al., 2013). Thus, an important MWR performance requirement is the capability for accurate upper-air thermodynamic surveillance in all weather conditions (Ware et al., 2013). Yet the MWR measurement technology is based on an indirect measurement and, as such, it is necessary to know the uncertainty of these measurements, especially in comparison with radiosonde. It is found in studies that since the measurement principles of MWRs and radiosonde are different (volume integral above a fixed location on the ground for MWRs vs. point measurement of a drifting balloon for radiosonde), there are biases and spreads of the data points, but the two data sets typically agree within the observation error assigned to radiosondes when they are assimilated into numerical weather models (Ware et al., 2003, 2013; Knupp et al., 2009; Cimini et al., 2011) and follow similar trends in the evolution of the temperature and humidity inside the troposphere (Güldner and Spänkuch, 2001; Chan and Hon, 2011; Madhulatha et al., 2013). Some studies show that a MWR is mainly suited for continuous observations in the low troposphere (Liu, 2011; Löhnert and Maier, 2012), and calibration corrections should be applied to reduce the system bias between MWR and radiosonde observations before obtaining the MWR potential benefits in operational activities (Calpini et al., 2011; Tan et al., 2011; Güldner, 2013; Sánchez et al., 2013).

Although a MWR has an advantage of high temporal resolution, it is mainly used in non-precipitation conditions because the radiometer measurements become less accurate in the presence of a water film on the outer housing (radome) of the equipment. Moreover, the radiometer retrieval normally does not include the scattering and emission/absorption effects of rain. Recently there are some progress in applying rain-effect mitigation methods to the radiometer, such as a hydrophobic radome and forced airflow over the radome surface (Chan, 2009). In addition, the Radiometrics Corporation retrieved temperature, humidity and liquid profiles from off-zenith (15° elevation) radiometer observations to provide higher accuracy during precipitation by minimizing the affect of liquid water and ice on the radiometer radome (Cimini et al., 2011; Ware et al., 2013). In this study, the impact of precipitation on MWR measurement accuracy is evaluated against radiosonde using a 3 year data set of MWR-retrieved temperature and humidity profiles with collocated vertical soundings of the atmosphere in Wuhan, China, and the effect of off-zenith observation on reducing the impact of precipitation is also explored.

2. Instruments and methods

Wuhan (30.6°N, 114.1°E, 23 m above sea level) is an operational radiosonde station in central China. A MWR was installed in Wuhan in June 2010. This paper focuses on the period from June 2010 to September 2013. The data used in this paper were collected by continuous MWR observations (at about 3-min intervals) and by radiosonde ascents (at 12-h intervals). The MWR is a Radiometrics MP-3000A unit, which observes 21 K-band (22–30 GHz) and 14 V-band (51–59 GHz) microwave channels at multiple elevation angles, one zenith infrared (9.6–11.5 μm) channel, and surface temperature, humidity and pressure sensors (Cimini et al., 2011; Ware et al., 2013). Vertical retrieval intervals are 50 m from the surface to 500 m, 100 m to 2 km, and 250 m to 10 km. To minimize such errors caused by liquid water on the MWR antenna radome, the radome is made hydrophobic to repel liquid water, and a special blower system is used to sweep water beads and snow away from the radome (Chan, 2009). A rain sensor is combined with the MWR, which is used to provide a "Rain Flag" for data that is potentially contaminated by some liquid water on the radome. The rain flag data is 0 (Rain = 0) and 1 (Rain = 1) in non-precipitation and precipitation conditions, respectively.

The MWR receives roughly a picowatt of Planck radiation emitted by atmospheric oxygen and water vapor molecules and liquid water, in multiple frequency channels. The atmosphere is semi-transparent in the K-band and lower V-band channels during non-precipitation conditions, receiving emission from the atmosphere in addition to cosmic background radiation. The microwave, infrared and surface meteorological observations are automatically converted into continuous temperature, humidity and liquid profiles using radiative transfer equations and neural networks. The neural

network retrieval method uses historical radiosondes to characterize states of the atmosphere that commonly occur at a particular location (Ware et al., 2013). A five-year data set of historical radiosondes in Wuhan was used for neural network training.

Heated forced air is commonly used to minimize accumulation of liquid water on radiometer radomes during precipitation. However, during heavy precipitation, and in particular in sub-freezing conditions, it is difficult to prevent accumulation of liquid water or ice on the radiometer radome. Although heated forced air can increase evaporation during light precipitation, it is relatively ineffective during heavy precipitation and may increase ice buildup during heavy sleet/snow conditions. In this study, MWR thermodynamic profiles are retrieved from zenith and off-zenith observations, respectively. In off-zenith method, MWR thermodynamic profiles are retrieved from off-zenith observations only (zenith observations are not included), in combination with unheated forced air and proprietary neural network retrieval methods (Cimini et al., 2011; Ware et al., 2013). The MWR observes at 15° elevation through vertical sections of the inverted "U" shaped radome that are more readily cleared of water droplets by gravity than the horizontal sections observed at zenith. Furthermore, at 15° elevation, K-band and lower V-band brightness temperatures are several times larger than those at zenith, further increasing signal to noise for off-zenith observations. In addition, the MWR hardware and software include patented rain effect mitigation methods (Ware et al., 2006).

Radiosondes launched from the Wuhan station are L-band radio sounding systems, providing vertical pressure, temperature, relative humidity, dew point temperature, and wind profiles at 1-s resolution. Two radiosonde soundings were obtained daily at standard synoptic hours of 00 and 12 UTC. The radiosonde profiles are used for comparison and validation of the MWR temperature and humidity profiles.

The MWR temperature and humidity profiles were retrieved from zenith observations during June 2010 to April 2013, which are used to compare with collocated radiosondes to evaluate the impact of precipitation on MWR measurement accuracy. During April to September in 2013, the MWR temperature and humidity profiles were retrieved from zenith and off-zenith (15° elevation) observations, respectively, and are used to explore the effect of off-zenith observation on reducing the impact of precipitation on MWR measurement accuracy. The MWR is calibrated by using liquid nitrogen in a top-mount target in each season, and the calibration accuracy is within 0.5 K. Since the radiosondes are launched twice at 00 and 12 UTC each day and the MWR profiles are retrieved at about 3-min intervals, only the MWR profiles closest in time of 00 and 12 UTC are used for comparison against the radiosonde ascent. To explore the MWR measurement accuracy on the whole, the MWR retrievals are firstly compared with the radiosondes without considering the level division in altitude, and then the discrepancy between the MWR retrievals and radiosondes along the altitude is performed to explore the variation of MWR measurement accuracy with altitude.

3. Impact of precipitation on MWR retrievals

To evaluate the impact of precipitation on MWR measurement accuracy, we compared the profiles of temperature, vapor density and relative humidity between the MWR and radiosonde in Wuhan during June 2010 to April 2013. The data set is divided into two samples of non-precipitation (Rain = 0) and precipitation (Rain = 1) conditions. As shown in Table 1, without considering the level division in altitude, the MWR temperature and vapor density profiles have a significant correlation with radiosondes in both non-precipitation and precipitation, with the correlation coefficients above 0.92. The correlation of relative humidity between the MWR and radiosonde is reasonable with a correlation coefficient of 0.77 and 0.68 in non-precipitation and precipitation, respectively. The MWR temperature has a cold bias of −1.9 K against radiosondes in non-precipitation, however, the MWR temperature bias becomes warm with 2.1 K in precipitation, and the root-mean-square (RMS, here means the standard deviation) between the MWR and radiosonde increases from 3.2 K to 5.3 K. The MWR vapor density has a wet bias against radiosondes, especially in precipitation. The vapor density bias between the MWR and radiosonde increases from 0.06 g/m^3 in non-precipitation to 1.31 g/m^3 in precipitation, with the corresponding RMS also increasing from 0.30 g/m^3 to 2.28 g/m^3. It is the same situation for the MWR relative humidity where the wet bias of the MWR relative humidity against radiosondes increases from 7% in non-precipitation to 10% in precipitation, with the corresponding RMS varying from 21% to 24%. It can be seen that the discrepancy between the MWR retrievals and radiosondes is larger in precipitation than in non-precipitation without considering the level division in altitude.

The discrepancy between the MWR retrievals and radiosondes along the altitude during non-precipitation and precipitation is also evaluated with the data set in Wuhan from June 2010 to April 2013. As shown in Fig. 1, the temperature correlation coefficient between the MWR and radiosonde is clearly smaller in precipitation than in non-precipitation below 8.75 km height, especially around 2 km height the correlation coefficient decreases from 0.95 to 0.70; however, above 8.75 km

Table 1
Comparison of MWR zenith retrievals against radiosondes without considering the level division in altitude during June 2010 to April 2013 in Wuhan.

Parameters	Rain flag	Numbers	Correlation coefficient	Bias	RMS
Temperature	Rain = 0	94 656	0.9876	−1.9 K	3.2 K
	Rain = 1	6960	0.9614	2.1 K	5.3 K
Vapor density	Rain = 0	94 656	0.9724	0.06 g/m^3	0.30 g/m^3
	Rain = 1	6960	0.9250	1.31 g/m^3	2.28 g/m^3
Relative humidity	Rain = 0	94 656	0.7721	7.3%	21.4%
	Rain = 1	6960	0.6752	9.9%	24.3%

height the precipitation shows no distinct impact on the temperature correlation coefficient. The MWR temperature shows a cold bias against radiosondes in non-precipitation, with a bias varying stably from about 0 K near the surface to −3.5 K at 10 km height, but in precipitation it is opposite below 8.75 km, the temperature bias increases from 0.5 K near the surface to 5.9 K at 2.25 km and then decreases to 0.2 K at 8.5 km before becoming cold with a value within 1 K. Furthermore, the temperature RMS between the MWR and radiosonde is significantly larger in precipitation than in non-precipitation. The temperature RMS increases from 1.1 K near the surface to 5.2 K at 10 km height in non-precipitation, but in precipitation it increases sharply from 1.0 K near the surface to 7.6 K at 1.8 km height and then decreases to 4.5 K at 3.5 km height before increasing again to 6.8 K at 10 km height.

Fig. 2 presents the comparison for vapor density profiles. It can be seen that the vapor density correlation coefficient between the MWR and radiosonde decreases with altitude in both non-precipitation and precipitation. The vapor density correlation coefficient is smaller in precipitation than in non-precipitation below 6.25 km, but it is opposite between 6.25 and 9.5 km. In non-precipitation, the MWR vapor density shows a dry bias against radiosondes below 1.6 km with a peak of −0.79 g/m^3 at 0.8 km height, while above 1.6 km the bias becomes wet with a peak of 0.74 g/m^3 at 4.0 km height. However, in precipitation the MWR vapor density shows a wet bias against radiosondes; it increases sharply from 0.24 g/m^3 near the surface to 3.32 g/m^3 at 2.0 km height and then decreases to the value of 0.08 g/m^3 at 10 km height. Although the precipitation shows no distinct impact on the MWR vapor density RMS below 0.5 km, the MWR vapor density RMS is clearly larger in precipitation than in non-precipitation above 0.5 km. Moreover, in both precipitation and non-precipitation, the MWR vapor density RMS varies with altitude in a similar pattern, in which the RMS firstly increases with altitude and then decreases with altitude before a maximum appearing at 1.6 km height. Most of the MWR vapor density RMS in non-precipitation is within 1.0 g/m^3 while that in precipitation is within 2.0 g/m^3, and the maximum RMS values appearing at 1.6 km height in non-precipitation and precipitation are 1.91 and 4.11 g/m^3, respectively.

Humidity measured by radiosondes and retrieved by the MWR is software-limited to 100% or less. If the raw humidity values exceed saturation they are truncated to saturation; this contributes to improved agreement during precipitating (saturated) conditions. Similar improved agreement during precipitation is previously reported (Japan Meteorological Agency, 2008). The comparison for relative humidity profiles is presented in Fig. 3. As the radiosonde and radiometer relative humidity profiles are artificially limited to not exceed 100%, differences between the two methods are limited and

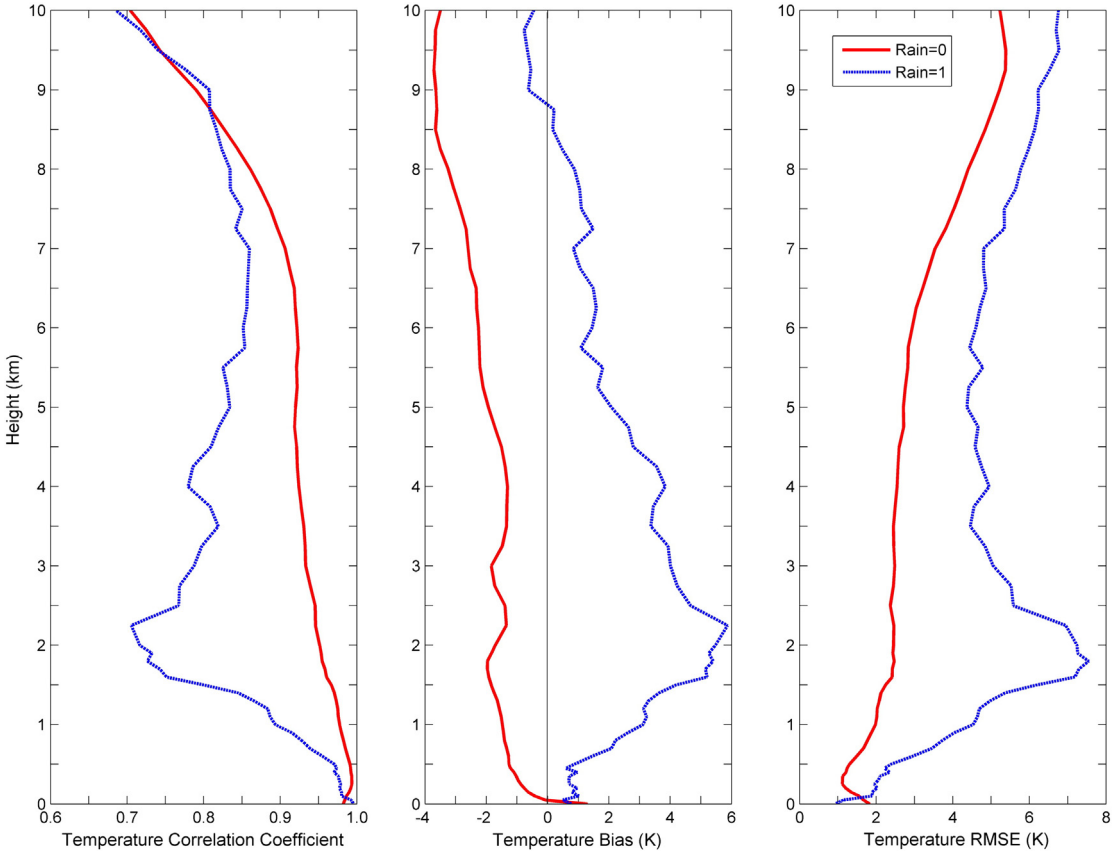

Fig. 1. The correlation coefficient, bias and RMS of temperature profiles between the MWR and radiosonde during non-precipitation (red solid line) and precipitation (blue dotted line) in Wuhan from June 2010 to April 2013. The profile cases in non-precipitation and precipitation are 1632 and 120, respectively. (For interpretation of the references to color in this figure legend, the reader is referred to the web version of this article.)

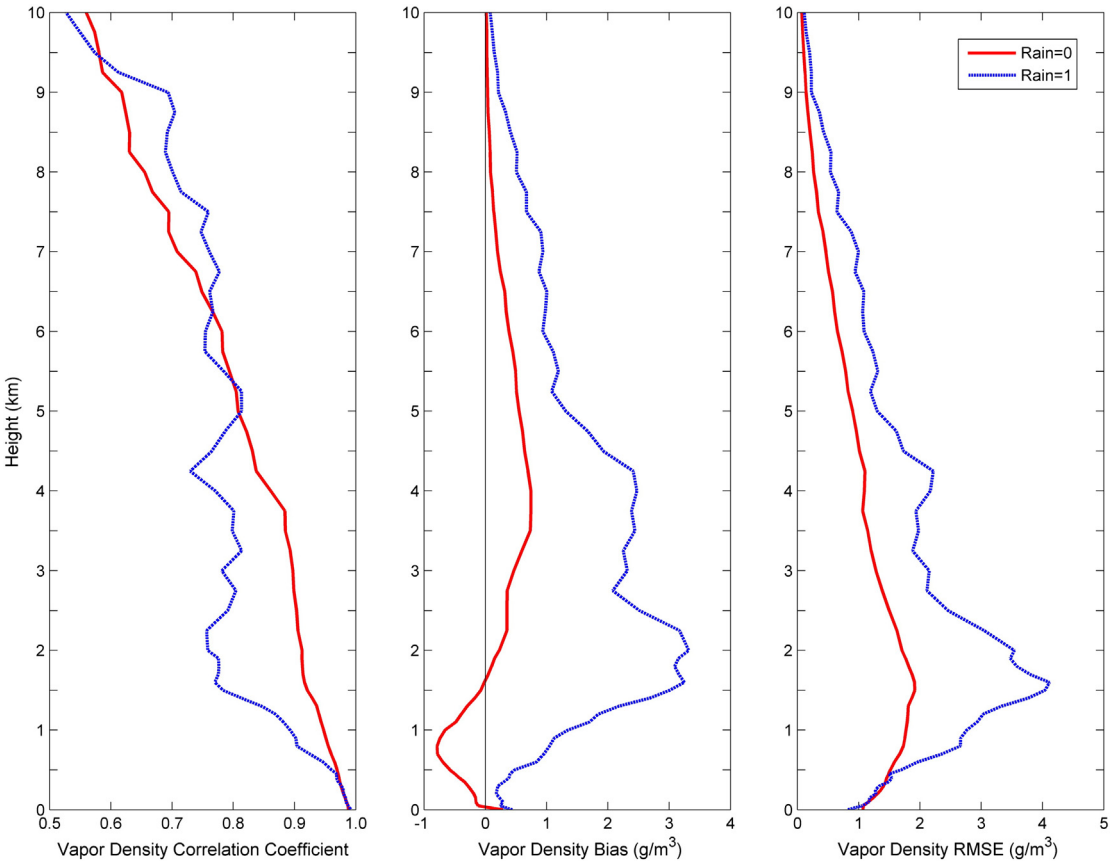

Fig. 2. Same as Fig. 1 but for vapor density profiles.

mixed in precipitating conditions close to saturation. The relative humidity correlation coefficient between the MWR and radiosonde is smaller in precipitation than in non-precipitation below 4.5 km, especially from the surface to 2 km, but the discrepancy is not distinct above 4.5 km. Excluding a dry bias of −2.1% at the surface level in non-precipitation, the MWR relative humidity shows a wet bias against radiosondes in both non-precipitation and precipitation. In non-precipitation, the MWR relative humidity bias firstly increases from 0.2% near the surface to 18.1% at 5.0 km and then decreases to 5.8% at 10 km, and in precipitation the MWR relative humidity bias increases with altitude in principle, varying from 0.2% at the surface to 27.4% at 10 km. However, the MWR relative humidity bias is smaller in precipitation than in non-precipitation below 5.25 km, but it is opposite above 5.25 km and the discrepancy between them enlarges with altitude. The MWR relative humidity RMS in non-precipitation increases generally with altitude, which varies from 9.7% at the surface to 22.7% at 10 km height with the maximum of 26.4% appearing at 5 km height. Although the MWR relative humidity RMS in precipitation also increases with altitude on the whole, a peak of 22.1% appears at 1.5 km height and the maximum of 33.7% appears at 9.0 km height. Moreover, the MWR relative humidity RMS is larger in precipitation than in non-precipitation below 1.7 km and above 5.25 km, but the former is smaller than the latter at 1.7–5.25 km heights.

In addition, excluding the correlation coefficient profiles in Fig. 2 and the RMS profiles in Fig. 3, the differences of the profiles in Figs. 1–3 between the precipitation and non-precipitation cases are at the 0.05 significance level with a t test.

4. Effect of off-zenith observation on MWR retrievals

The MWR profiles are retrieved from the simultaneous zenith and off-zenith observations during May to September 2013 in Wuhan. To explore the effect of off-zenith observation on MWR measurement accuracy, the coupled MWR zenith and off-zenith retrievals around the time of 00 and 12 UTC are compared with the collocated radiosondes. Table 2 presents the comparison of MWR zenith and off-zenith retrievals against radiosondes without considering the level division in altitude. It can be seen that in non-precipitation the MWR temperature cold bias and RMS against radiosondes are smaller in off-zenith than in zenith, and in precipitation the MWR temperature warm bias is reduced from 3.6 K in zenith to 1.3 K in off-zenith, with the RMS also reducing from 4.2 K to 3.1 K. For vapor density, the MWR bias against radiosondes in non-precipitation is slightly larger in off-zenith than in zenith with a very close RMS, and in precipitation the MWR bias is reduced from 1.10 g/m^3 in zenith to 0.18 g/m^3 in off-zenith, with the RMS also reducing from 2.90 g/m^3 to 1.91 g/m^3. Although the MWR relative humidity bias against radiosondes in non-precipitation is slightly smaller

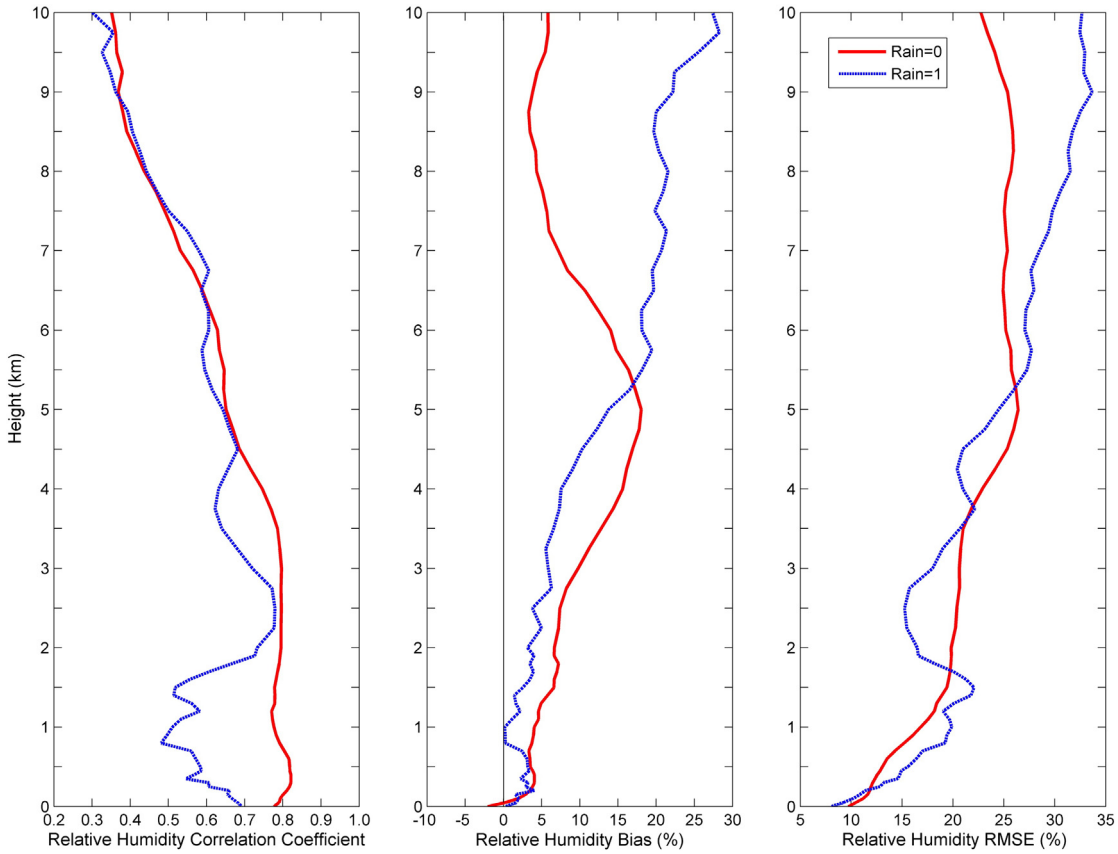

Fig. 3. Same as Fig. 1 but for relative humidity profiles.

in off-zenith than in zenith with a same RMS, the discrepancy of MWR relative humidity against radiosondes in precipitation varies from a wet bias of 3.9% in zenith to a dry bias of −12.1% in off-zenith, and the corresponding RMS also increases slightly. Once again, it should be taken into consideration that radiosonde and radiometer relative humidities are artificially limited to less than 100% which may improve agreement between the two methods during precipitating, saturated conditions. In addition, the correlation coefficients between the MWR retrievals and radiosondes in precipitation are larger in off-zenith than in zenith, especially for vapor density where it increases from 0.91 to 0.97.

The impact of off-zenith observation on MWR measurement accuracy is also explored in considering the level division in altitude. Fig. 4 presents the comparison of MWR temperature profiles against radiosondes in zenith and off-zenith observations during May to September 2013 in Wuhan. It can be seen that in non-precipitation the temperature correlation coefficient between the MWR and radiosonde is larger in off-zenith observation than in zenith observation below 5.5 km and

Table 2
Comparison of MWR zenith and off-zenith retrievals against radiosondes without considering the level division in altitude during May to September 2013 in Wuhan.

Parameters	Rain flag	Observation mode	Numbers	Correlation coefficient	Bias	RMS
Temperature	Rain = 0	Zenith	14 500	0.9911	−2.4 K	2.8 K
	Rain = 0	Off-zenith	14 500	0.9936	−1.1 K	2.1 K
	Rain = 1	Zenith	928	0.9678	3.6 K	4.2 K
	Rain = 1	Off-zenith	928	0.9831	1.3 K	3.1 K
Vapor Density	Rain = 0	Zenith	14 500	0.9763	0.12 g/m^3	1.62 g/m^3
	Rain = 0	Off-zenith	14 500	0.9792	0.37 g/m^3	1.61 g/m^3
	Rain = 1	Zenith	928	0.9069	1.10 g/m^3	2.90 g/m^3
	Rain = 1	Off-zenith	928	0.9657	0.18 g/m^3	1.91 g/m^3
Relative Humidity	Rain = 0	Zenith	14 500	0.7713	7.4%	19.4%
	Rain = 0	Off-zenith	14 500	0.7759	6.3%	19.4%
	Rain = 1	Zenith	928	0.5648	3.9%	20.3%
	Rain = 1	Off-zenith	928	0.6021	−12.1%	22.0%

above 8.75 km, and it is opposite during 5.5–8.75 km heights. Although in non-precipitation the MWR temperature bias in off-zenith observation shows no distinct difference from that in zenith observation below 2.0 km, the cold temperature bias above 2.0 km is clearly reduced in off-zenith observation, with the peak bias varying from −4.7 K to −2.2 K. Moreover, the MWR temperature RMS in non-precipitation is obviously smaller in off-zenith compared to zenith observations, which ranges 1.0–2.6 K and 1.8–3.3 K, respectively. In precipitation, the temperature correlation coefficient between the MWR and radiosonde in off-zenith observation is slightly smaller than that in zenith observation below 2.5 km, but the former is clearly larger than the latter above 2.5 km. The MWR warm temperature bias in precipitation is also clearly reduced in off-zenith observation, which varies in −0.2–3.1 K and that for zenith observation is 1.5–8.3 K. The MWR temperature RMS in precipitation shows no distinct difference in zenith and off-zenith observations below 2.5 km, but it is clearly smaller in off-zenith observation than in zenith observation above 2.5 km, with a peak reducing from 6.8 K to 3.7 K.

As shown in Fig. 5, in non-precipitation the vapor density correlation coefficient between the MWR and radiosonde in off-zenith observation shows no distinct difference from that in zenith observation below 1.5 km, but the former is slightly larger than the latter above 1.5 km. For the MWR vapor density bias in non-precipitation, it is wet against radiosondes below 1.0 km and above 4.0 km but dry at other heights in zenith observation; in off-zenith observation, the wet bias becomes larger below 1.0 km while smaller above 5.0 km, and the dry bias becomes smaller at 1.8–2.75 km heights while larger at 2.75–4.0 km heights, but at the other heights the bias signs in zenith and off-zenith observations are opposite. Same as the correlation coefficient, the MWR vapor density RMS in non-precipitation shows no distinct difference between off-zenith and zenith observations below 2 km, but above 2 km the MWR vapor density RMS is smaller in off-zenith observation than in zenith observation, and it is more obvious at 2–5 km heights. In precipitation, the vapor density correlation coefficient between the MWR and radiosonde in off-zenith observation is smaller than that in zenith observation below 2 km, but the former is clearly larger than the latter above 2 km, with most values increasing from below 0.4 to above 0.5. The MWR vapor density in precipitation mainly shows a dry bias against radiosondes in zenith observation below 1.6 km while a wet bias above 1.6 km; although in off-zenith observation the MWR vapor density bias sign is opposite to that in zenith observation at most heights, the bias range is significantly reduced from −2.34–6.04 g/m^3 to −1.17–1.42 g/m^3. For the MWR vapor density RMS in precipitation, it is larger in off-zenith observation than in zenith observation below 1.8 km, but the former is clearly

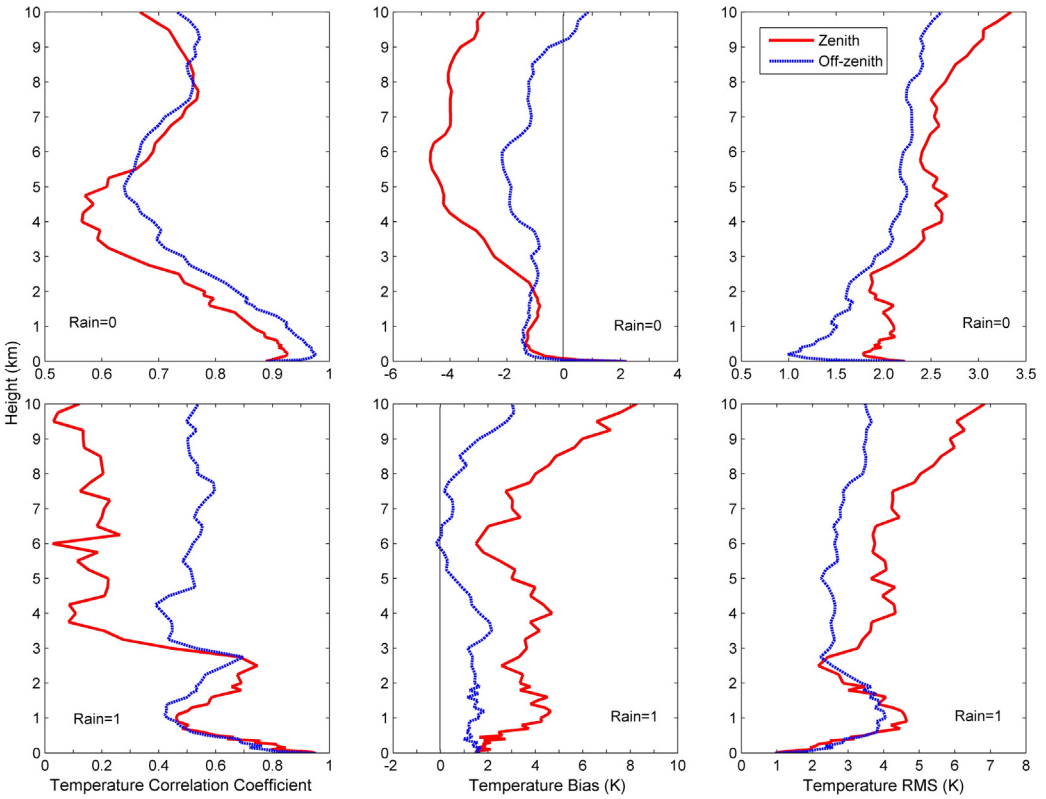

Fig. 4. The correlation coefficient, bias and RMS of temperature profiles between the MWR and radiosonde in zenith (red solid line) and off-zenith (blue dotted line) observations during May to September 2013 in Wuhan. The upper panel is for non-precipitation, and the lower panel is for precipitation. The profile cases in non-precipitation and precipitation are 250 and 16, respectively. (For interpretation of the references to color in this figure legend, the reader is referred to the web version of this article.)

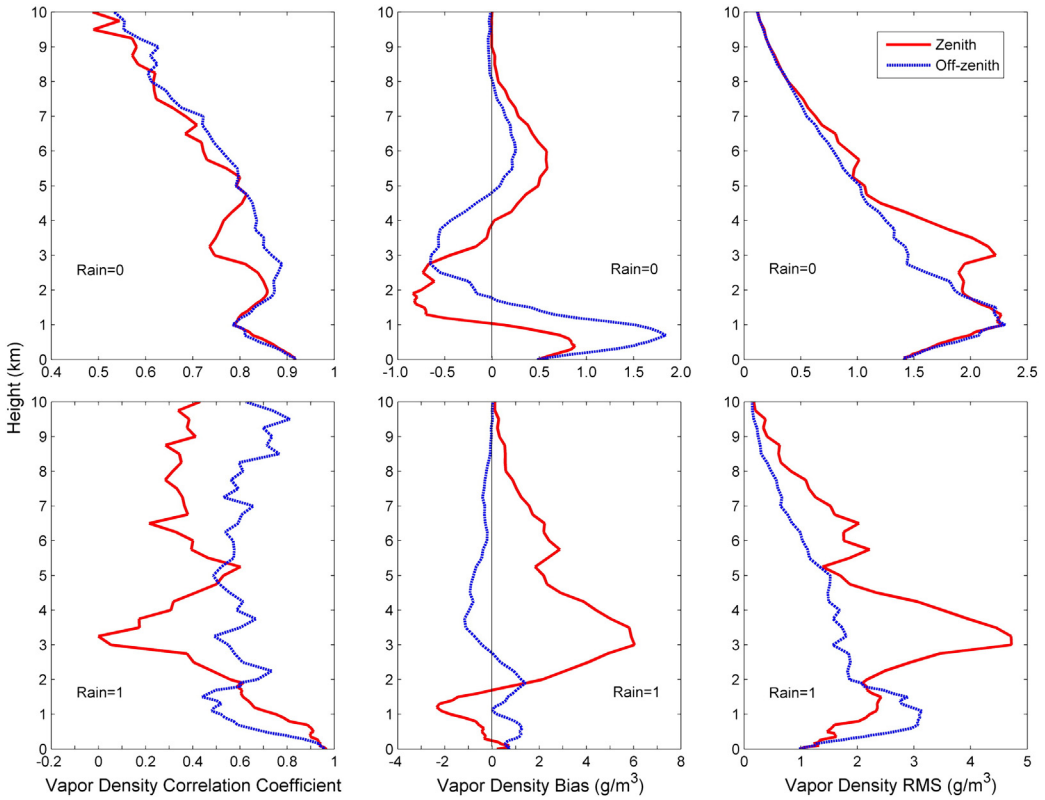

Fig. 5. Same as Fig. 4 but for vapor density profiles.

smaller than the latter above 1.8 km especially at 1.8–5.0 km heights, and the maximum RMS is also reduced from 4.72 g/m^3 in zenith observation to 3.14 g/m^3 in off-zenith observation.

The comparison of MWR relative humidity profiles against radiosondes in zenith and off-zenith observations is presented in Fig. 6. In non-precipitation, except above 7 km, the relative humidity correlation coefficient between the MWR and radiosonde in off-zenith observation is slightly smaller than that in zenith observation, and the discrepancy between them shows no distinct difference at other heights. For the MWR relative humidity bias in non-precipitation, it is dry against radiosondes near the surface but wet at other heights in zenith observation; while in off-zenith observation, the wet bias increases below 2 km but decreases above 4.75 km, and at the other heights the bias changes its sign with a close magnitude. Moreover, the MWR relative humidity bias ranges in −5%–21% in zenith observation, and in off-zenith observation it is −6%–14%. Same as the correlation coefficient, the MWR relative humidity RMS in non-precipitation shows no distinct difference between off-zenith and zenith observations below 7.5 km, except that the former is slightly larger than the latter above 7.5 km. In precipitation, the relative humidity correlation coefficient between the MWR and radiosonde is smaller in off-zenith observation than in zenith observation at most heights below 9 km, while it is opposite above 9 km. Note that a negative correlation coefficient appears at 3 km in zenith observation but it changes to positive in off-zenith observation. For the MWR relative humidity bias in precipitation, it is dry against radiosondes below 1.5 km and at 3.5–5.5 km heights but wet at the other heights in zenith observation; however, it is dry at most heights except a little wet around 2.5 km height in off-zenith observation, and the bias range is −29%–1% smaller than the range of −12%–31% in zenith observation. Although the MWR relative humidity RMS in precipitation is slightly smaller in off-zenith observation than in zenith observation above 8.5 km, the former is larger than the latter below 8.5 km especially at 4–6 km heights.

5. Discussions and conclusions

MWRs can be useful for the detection of mesoscale phenomena because of its ability to obtain constant continuous measurements of temperature and humidity profiles. These profiles are mainly used in non-precipitation conditions because the MWR measurements become less accurate in the presence of a water film on the radome of the equipment. Recently, there have been improvements in applying rain-effect mitigation methods to the radiometer, such as a hydrophobic radome and forced airflow over the radome surface. In addition, Radiometrics Corporation retrieved the temperature and humidity profiles from off-zenith (15° elevation) radiometer observations to provide higher accuracy during precipitation by minimizing the affect of liquid water and ice on the radiometer radome.

In this paper, the impact of precipitation on the MWR measurement accuracy against radiosonde is evaluated using a 3 year data set of MWR-retrieved temperature and humidity profiles with collocated radiosondes in Wuhan. Without considering the level division in altitude, the MWR retrievals still have reasonable correlation coefficients with radiosondes in precipitation. However, the MWR retrieval

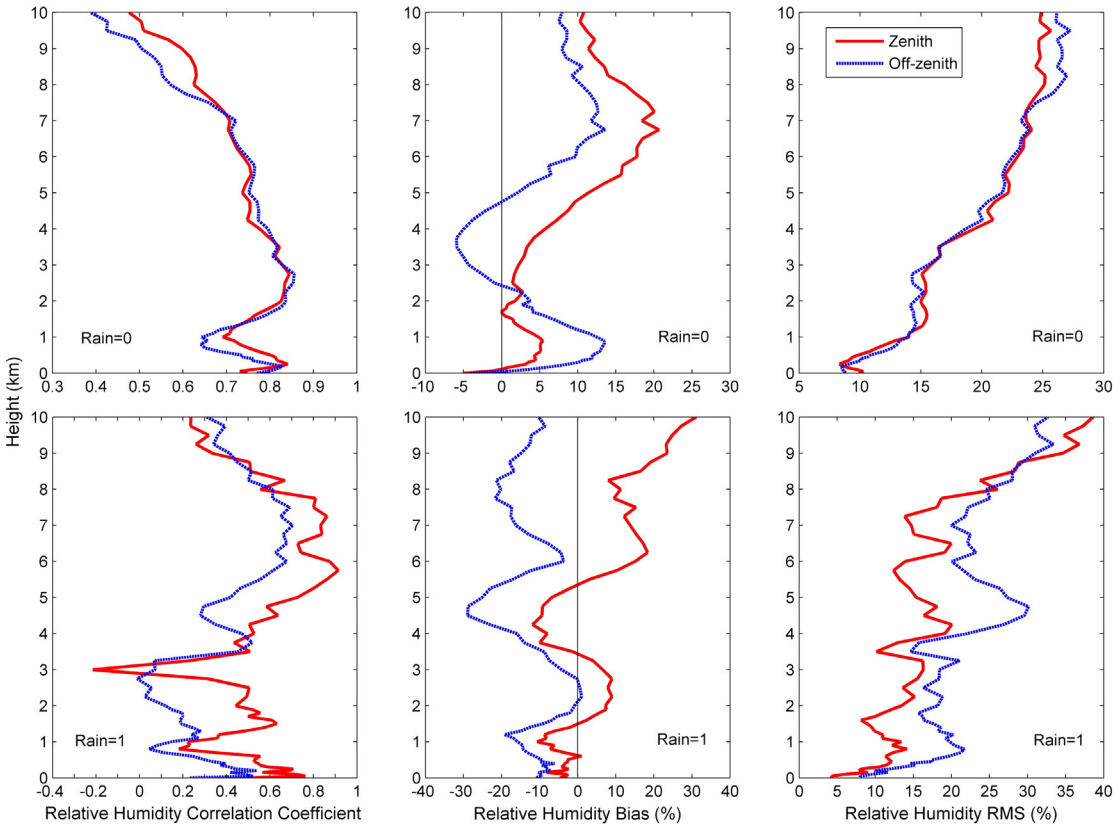

Fig. 6. Same as Fig. 4 but for relative humidity profiles.

accuracy against radiosondes in precipitation is not good as that in non-precipitation, and the absolute biases for the temperature, vapor density and relative humidity are 2.1 K, 1.31 g/m^3 and 10%, with the corresponding RMS errors of 5.3 K, 2.28 g/m^3 and 24%, respectively. Considering the level division in altitude, the MWR temperature is mostly impacted by precipitation around 2 km height compared with the results in non-precipitation, at which the correlation coefficient decreases from 0.95 to 0.70 while the absolute bias and RMS error increase from 1.4 and 2.5 K to 5.9 and 7.6 K, respectively. The impact of precipitation on the MWR vapor density is also most obvious around 2 km height, at which the correlation coefficient, absolute bias and RMS error vary from 0.91, 0.23 g/m^3 and 1.91 g/m^3 in non-precipitation to 0.76, 3.32 g/m^3 and 4.11 g/m^3 in precipitation, respectively. For the MWR relative humidity, the correlation coefficient in precipitation is obviously smaller than that in non-precipitation below 4.5 km, and the absolute bias and RMS error are clearly larger above 5.5 km. Additionally, the differences between the precipitation and non-precipitation cases mostly are statistically significant.

The effect of off-zenith observation on reducing the impact of precipitation on MWR measurement accuracy is explored in this paper by comparing the MWR retrievals in zenith and off-zenith observations with collocated radiosondes. Without considering the level division at altitude, the off-zenith observation makes a positive effect on reducing the impact of precipitation on the accuracy of MWR temperature and vapor density retrievals. The MWR temperature bias against radiosondes is reduced from 3.6 K in zenith observation to 1.3 K in off-zenith observation, with the RMS error also reducing from 4.2 K to 3.1 K. For the MWR vapor density, the bias and RMS error are reduced from 1.10 g/m^3 and 2.90 g/m^3 in zenith observation to 0.18 g/m^3 and 1.91 g/m^3, respectively. Although the relative humidity correlation coefficient between the MWR and radiosonde is slightly larger in off-zenith observation than in zenith observation, the former's bias of −12% is larger than the latter's bias of 4% with close RMS errors. Considering the level division at altitude, the temperature correlation coefficient between the MWR and radiosonde in precipitation conditions is clearly improved in off-zenith observation above 3 km heights, and the temperature warm bias against radiosondes is also significantly reduced from the surface to 10 km with a distinct smaller RMS error above 3 km. For the MWR vapor density retrievals in precipitation, the correlation coefficient and RMS error against radiosondes are also improved in off-zenith observation above 2 km, and the bias is also clearly reduced at most heights. However, the relative humidity correlation coefficient between the MWR and radiosonde in precipitation is only improved in off-zenith observation around 3 km height, and the relative humidity bias range is just reduced from −12%–31% to −29%–1% with the RMS error only reduced above 8.5 km. Additionally, the off-zenith observation also makes a positive effect on the MWR measurement accuracy in non-precipitation conditions, especially for the temperature and vapor density profiles at most heights, and this result is better than that given by Güldner (2013), in which the off-zenith observation improves the accuracy of MWR temperature and vapor density retrievals in the boundary layer.

Our results suggest that the off-zenith observation makes a positive effect on reducing the impact of precipitation on the accuracy of the MWR temperature and vapor density profiles. The MWR temperature profile retrieved from off-zenith observation in precipitation has a reasonable accuracy against radiosondes, which is comparable to the result of zenith observation in non-precipitation. Moreover, the accuracy of the MWR vapor density profile retrieved from off-zenith observation is also generally better than that from zenith observation in precipitation. However, the effect of off-zenith observation on reducing the impact of precipitation on the MWR relative humidity accuracy is not obvious like those for the MWR temperature and vapor density profiles. Note that MWR and radiosonde relative humidities are both at a cutoff of 100% in software. Both are likely to saturate when heavy rain soaks the radiosonde humidity sensor and the MWR brightness temperature is augmented by scattering from large hydrometeors. This may partly explain the larger differences between zenith and off-zenith temperature and vapor density retrievals compared to relative humidity retrievals. Furthermore, the results also indicate that the off-zenith observations during non-precipitation cases are better compared with zenith observations. Therefore, in general off-zenith observations are better than zenith observations. This could be due to the fact that the off-zenith observations are more representative of the conditions in which radiosonde observations are also taken.

Acknowledgments

This work was supported by the National High Technology Research and Development Program ("863" Program) of China (grant no. 2012AA120902), the open project of State Key Laboratory of Severe Weather, Chinese Academy of Meteorological Sciences (grant no. 2013LASW-A02), and the National Natural Science Foundation of China (grant nos. 41175016 and 41375041). The authors would like to appreciate the reviewers for their valuable comments in improving the quality of this paper.

References

Cadeddu, M.P., Liljegren, J.C., Turner, D.D., 2013. The atmospheric radiation measurement (ARM) program network of microwave radiometers: instrumentation, data, and retrievals. Atmos. Meas. Tech. 6, 2359–2372.

Calpini, B., Ruffieux, D., Bettems, J.-M., Hug, C., Huguenin, P., Isaak, H.-P., Kaufmann, P., Maier, O., Steiner, P., 2011. Ground-based remote sensing profiling and numerical weather prediction model to manage nuclear power plants meteorological surveillance in Switzerland. Atmos. Meas. Tech. 4, 1617–1625.

Chan, P.W., 2009. Performance and application of a multi-wavelength, ground-based microwave radiometer in intense convective weather. Meteorol. Z. 18, 253–265.

Chan, P.W., Hon, K.K., 2011. Application of ground-based, multi-channel microwave radiometer in the nowcasting of intense convective weather through instability indices of the atmosphere. Meteorol. Z. 20, 423–429.

Cimini, D., Campos, E., Ware, R., Albers, S., Graziano, G., Oreamuno, J., Joe, P., Koch, S., Cober, S., Westwater, E., 2011. Thermodynamic atmospheric profiling during the 2010 Winter Olympics using ground-based microwave radiometry. IEEE Trans. Geosci. Remote Sens. 49, 4959–4969.

Güldner, J., 2013. A model-based approach to adjust microwave observations for operational applications: results of a campaign at Munich airport in winter 2011/2012. Atmos. Meas. Tech. 6, 2879–2891.

Güldner, J., Spänkuch, D., 2001. Remote sensing of the thermodynamic state of the atmospheric boundary layer by ground-based microwave radiometry. J. Atmos. Ocean. Technol. 18, 925–933.

Huang, Z., Xu, G., Wang, X., Tang, Y., 2013. Applications of ground-based microwave radiation data to short-term rainstorm and potential forecast. J. Appl. Meteorol. Sci. 24, 576–584 (in Chinese).

Japan Meteorological Agency, 2008. Improved 1D-Var assimilation retrieval of temperature and humidity from the ground-based microwave radiometer data. Observations Department Special Report.

Knupp, K., Ware, R., Cimini, D., Vandenberghe, F., Vivekanandan, J., Westwater, E., Coleman, T., 2009. Ground-based passive microwave profiling during dynamic weather conditions. J. Atmos. Ocean. Technol. 26, 1057–1073.

Liu, H., 2011. The temperature profile comparison between the ground-based microwave radiometer and the other instrument for the recent three years. Acta Meteorol. Sin. 69, 719–728 (in Chinese).

Liu, H., Wang, Y.C., Wang, J., Li, J., Cao, X., Xiong, B., 2009. Preliminary analysis of the characteristics of precipitable water vapor measured by the ground-based 12-channel microwave radiometer in Beijing. Chin. J. Atmos. Sci. 33, 388–396 (in Chinese).

Löhnert, U., Maier, O., 2012. Operational profiling of temperature using ground-based microwave radiometry at Payerne: prospects and challenges. Atmos. Meas. Tech. 5, 1121–1134.

Madhulatha, A., Rajeevan, M., Ratnam, M.V., Bhate, J., Naidu, C.V., 2013. Nowcasting severe convective activity over southeast India using ground-based microwave radiometer observations. J. Geophys. Res. 118, 1–13.

Raju, C.S., Renju, R., Antony, T., Mathew, N., Moorthy, K.K., 2013. Microwave radiometric observation of a waterspout over coastal Arabian Sea. IEEE Trans. Geosci. Remote Sens. http://dx.doi.org/10.1109/LGRS.2012.2229960.

Sánchez, J.L., Posada, R., Garcia-Ortega, E., Lopez, L., Marcos, J.L., 2013. A method to improve the accuracy of continuous measuring of vertical profiles of temperature and water vapor density by means of ground-based microwave radiometer. Atmos. Res. 122, 43–54.

Spänkuch, D., Güldner, J., Steinhagen, H., Bender, M., 2011. Analysis of a drylin-like feature in northern Germany detected by ground-based microwave profiling. Meteorol. Z. 20, 409–421.

Tan, H., Mao, J., Chen, H., Chan, P.W., Wu, D., Li, F., Deng, T., 2011. A study of a retrieval method for temperature and humidity profiles from microwave radiometer observations based on principal component analysis and stepwise regression. J. Atmos. Ocean. Technol. 28, 378–389.

Tang, R., Li, D., Xiang, Y., Xu, G., Li, Y., Chen, Y., 2012. Analysis of a hailstorm event in the middle Yangtze River basin using ground microwave radiometers. Acta Meteorol. Sin. 70, 806–813 (in Chinese).

Venkat Ratnam, M., Durga Santhi, Y., Rajeevan, M., Vijaya Bhaskara Rao, S., 2013. Diurnal variability of stability indices observed using radiosonde observations over a tropical station: comparison with microwave radiometer measurements. Atmos. Res. 124, 21–33.

Ware, R., Carpenter, R., Güldner, J., Liljegren, J., Nehrkorn, T., Solheim, F., Vandenberghe, F., 2003. A multi-channel radiometric profiler of temperature, humidity and cloud liquid. Radio Sci. 38 (4), 8079. http://dx.doi.org/10.1029/2002RS002856.

Ware, R., Solheim, F., Exner M., 2006. Precipitation effects mitigation at antenna systems, U.S. Patent #7, 145, 499.

Ware, R., Cimini, D., Campos, E., Giuliani, G., Albers, S., Nelson, M., Koch, S.E., Joe, P., Cober, S., 2013. Thermodynamic and liquid profiling during the 2010 Winter Olympics. Atmos. Res. 132–133, 278–290.

Xie, Y., Koch, S., McGinley, J., Albers, S., Bieringer, P., Woflson, M., Chan, M., 2011. A space-time multiscale analysis system: a sequential variational analysis approach. Mon. Weather Rev. 139, 1224–1240.